Int. J. Electrochem. Sci., 12 **(2017)** 7457 – 7468, doi: 10.20964/2017.08.55

International Journal of
ELECTROCHEMICAL
SCIENCE
www.electrochemsci.org

Xanthan Gum as a Potential Binder for Graphite Anode in Lithium-Ion Batteries

Zhaoqing Wang[1], *Guoju Dang*[1,2], *Quansheng Zhang*[1,*], *Jingying Xie*[2,3,*]

[1] Department of Chemical Engineering, Shanghai Institute of Technology, Shanghai 200235, China
[2] Shanghai Institute of Space Power Sources, Shanghai 200245, China
[3] Shanghai Power & Energy Storage Battery System Engineering Tech. Co. Ltd., Shanghai 200240, China
[*]E-mail: zhangquansheng@sit.edu.cn, jyxie@mail.sim.ac.cn

Received: 14 May 2017 / *Accepted:* 18 June 2017 / *Published:* 12 July 2017

As an important component of the electrode, the choice of appropriate and favorable binder is significant for fabricating lithium-ion (Li-ion) batteries with good cycle stability and C-rates capacity, which are implemented for numerous applications especially in portable electronics and eco-friendly electric vehicles (EV). In this work, xanthan gum was used as binder for graphite anode, the adhesive strength of the active materials to the current collector was investigated by scratch test. The results confirmed that the xanthan gum (XG) had a better bonding performance with copper (Cu) foil than poly (vinylidene fluoride) (PVDF), as well as XG had a larger plastic deformation resistance than the PVDF. Electrochemical impedance spectroscopy (EIS) measurement demonstrated that the graphite electrode using XG as binder has lower charge transfer resistance and more active kinetics on the electrode/electrolyte surface. All the electrochemical performance tests indicated that XG binder for graphite anode in Li-ion battery had a better cycling and rate performance than PVDF binder for graphite anode in Li-ion battery.

Keywords: scratch test, xanthan gum, electrochemical performance, graphite anode, Li-ion battery.

1. INTRODUCTION

Lithium-ion (Li-ion) battery has been one of the most promising electrochemical energy storage technologies based on the high-power density, energy density and long term duration [1-3], which is implemented for numerous applications especially in portable electronics and eco-friendly electric vehicles (EV). As an important component of the electrode, binder plays a significant role in the improvement of the performance of Li-ion batteries. Especially for anodes, the binder with good performance not only offers good adhesion between the active materials and the current collector, but

also can alleviate the swell of active particles attributed to the lithium-ion insert/deinsert into the active material layers. As is known to all, poly (vinylidene fluoride) (PVDF) has been a conventional binder because of good binding capacity, electrochemical stability and ability to absorb electrolyte [4-6]. However, more and more water-soluble binders are investigated to replace the PVDF binder since the water-soluble binder system is cheaper and more eco-friendly, as well as the Li-ion batteries fabricated with water-soluble binder show higher initial columbic efficiency, better cycle stability and C-rates capacity, e.g. sodium carboxymethyl cellulose (CMC), styrene butadiene rubber (SBR) and their mixture [7-9], CMC-formate [10], alginate [11], poly (acrylicacid-acrylonitrile-butylacrylate)-polystyrene [12], polyacrylic acid (PAA) [13], polyvinyl alcohol (PVA) [14], poly vinyl acetate (PVAc) [15], polyethylene mine (PEI) [16], polyimide (PI) [17], chitosan [18], polymerized vinylene carbonate (polyVC) [19], guar gum (GG) [20, 21]. It is important to find why the water-based Li-ion batteries show better electrochemical performance than PVDF-based Li-ion batteries.

Binder system for high-capacity electrodes should be able to provide: (1) inherent electronic conductivity under the Li-ion battery environment, (2) mechanical adhesion and ductility with inexhaustible tolerance of large volume change, and (3) electrolyte uptake to warrant high ionic conductivity [22]. Several methods have been used to evaluate the binder system. Peeling strength test has been used to evaluate the adhesion strength of the activity materials with current collector [23-26]. Tensile strength test has been applied to evaluate the adhesive force by investigating the stress of binder films along with different strains [27, 28]. Break stress test has been used assess the break stress of binder/conductive additive composite film with different binder/conductive additive weight ratios [29]. Scratch test, a significant mechanical test method that frequently being used in coating area, has been also conducted at the surface of electrodes to reveal the mechanical response for electrodes and evaluate the adhesion strength of a sliding surface [30-32], and just as the aforementioned investigations pointed, a scratch test simulates the stress induced by the volume change of the electrode active material, and the coefficient of friction (COF) can reflect the composite nature of the electrode and the mechanical properties of the polymer binder. And Sanjay Ramdon [33] investigated the mechanisms that cause reduced battery capacity with aging with mechanical integrity studies concluding nanoscratch, nanowear and nanofriction experiments. Scratch test can characterize the coating mechanical properties containing adhesive, hardness, elastic modulus, wear, coefficient of friction etc [34-37]. It is obviously to note that a flexible and ductile binder is more suitable for electrode in Li-ion battery than a rigid binder as it can buffer the volume expansion and good cohesion strength between binder and current collector can suppress active material fall off the current collector during the charge/discharge process. Swell test has been used to study the behavior when the binder film is immersed in the electrolyte [38-40], which demonstrates that it is necessary for the migration of lithium ion through the electrode particle/binder interface. However, the larger amounts of electrolyte uptake, the worse adhesive strength is between the binder with current collector. An outstanding binder can offer good electrolyte uptake capability to improve lithium ion migration without little weakened adhesive strength. Xanthan gum (XG) was reported in references [41-44] as lithium-ion battery binder, the results shown that the XG binder improved cycling and rate performance compared with CMC, PVDF. In this paper, scratch test was used to assess the binding mechanism of adhesion between the binders and Cu-current collector which results proved the better binding affinity of XG than PVDF,

and the EIS test shown the good electronic and ionic conductivity of graphite anode with XG binder, we prove that the electrochemical performance of graphite anode can be significantly improved with XG as a novel binder.

2. EXPERIMENTAL

2.1. Materials

Natural graphite (NG, Sinopharm Chemical Reagent Co., Ltd) was applied as the electrode active material. Acetylene black (AB) was used as the conductive additives, which was obtained from TIMCAL.XG, dispersed into deionized water with a concentration of 1wt% and purchased from Deosen Biochemical Ltd., was used as the binder. For comparison, PVDF (900 ，Arkema) binder was dissolved into NMP (Sinopharm Chemical Reagent Co., Ltd) with a concentration of 8 wt%. The electrolyte was 1.2M $LiPF_6$ in ethylene carbonate/ethyl methyl carbonate (EC/EMC, 1:1, v/v) supplied from Zhang jiagang Guotai-Huarong New Chemical Materials Co., Ltd..

2.2. Mechanical scratch test study

The adhesion between the binders and copper (Cu) foil current collector was investigated by a micro-scratch test on CETR UMT multi-functional tribometer at room temperature and 50-60% humidity, with a diamond tip used as the counterpart. The XG and PVDF binders' solutions were coated equably on the Cu foil with a doctor-blade (thickness 200um). After drying, these films were cut into specimens with an area of 1cm×2cm. The indenter scratched over the coating surface under a preload with 0.05N for 5s, and then a linear load from 0.05N to 5N at a constant sliding speed of 0.04mm/s and the total slide distance was 8mm. All the surface morphologies of PVDF/Cu (Cu substrate of PVDF based coating) and XG/Cu (Cu substrate of XG based coating) coatings after wear tests were observed by scanning electron microscopy (SEM, Hitachi S-3400N, 15kV).

2.3. Electrode preparation

For the preparation of the anode, slurry consisting of 94 wt% graphite powders and 6 wt% XG was stirred in a glass bottle for 24h with magnetic stirring. As a contrast, the anode using PVDF as another binder was prepared by coating the slurry containing 88.8 wt% graphite, 3.2wt% AB and 8 wt% PVDF. Then each paste was casted onto a 14 um-thick Cu foil (99.9% purity) using doctor blade technique (thickness 200 um). The obtained anodes were dried at 120℃ in a vacuum oven for 12h and pressed to enhance the contact between the electrode laminate and current collector. The electrodes were punched in 19mm diameter circle and dried at 120℃ under vacuum overnight. All the materials were stored at 60℃ before use. For half-cell test, the electrodes were assembled in a coin-type cell (CR2016) in an argon-filled glove box with metallic lithium as reference and counter electrodes, and a polypropylene film (Celgard 2400) as separator.

2.3. Electrode characterization

Cyclic voltammetry (CV) and Electrochemical impedance spectroscopy (EIS) measurements were performed using an electrochemical workstation at the room temperature. The cyclic voltammograms were measured at the scan rate of $0.1mV \cdot s^{-1}$ between the potential of 0.0V and 2.0V (vs. Li/Li^+). The EIS spectra were recorded in the frequency range from 10^{-2} to 10^5 Hz after different cycling stages.

The charge-discharge cycle tests and rate tests were performed with a battery charging-discharging instrument (from Wuhan LAND electronics Co., Ltd.) between 0.5mV and 2.0V (vs. Li/Li^+) at the room temperature. The cycle tests were carried out with a constant current of 0.5C (1C=372mAh g^{-1}). And the cells were charged (intercalation) at 0.2C and discharged (deintercalation) at different C-rates.

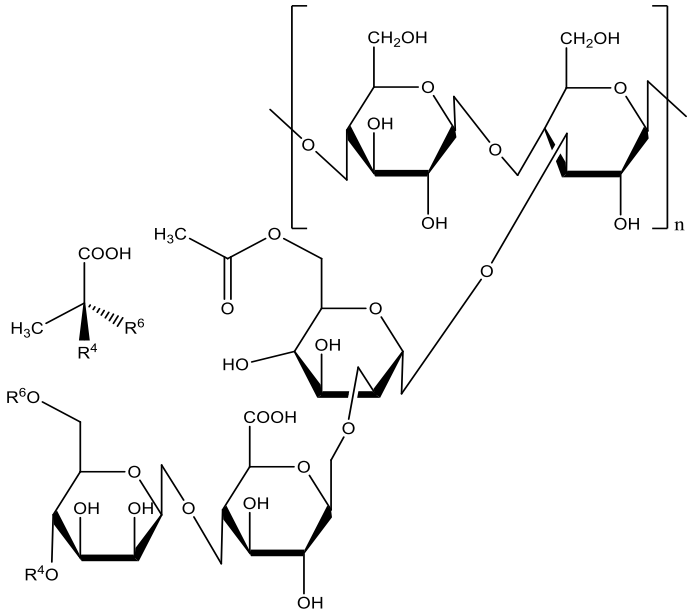

Figure 1. The molecular structure of xanthan gum polymer.

3. RESULTS AND DISCUSSION

3.1. Scratch test experiment

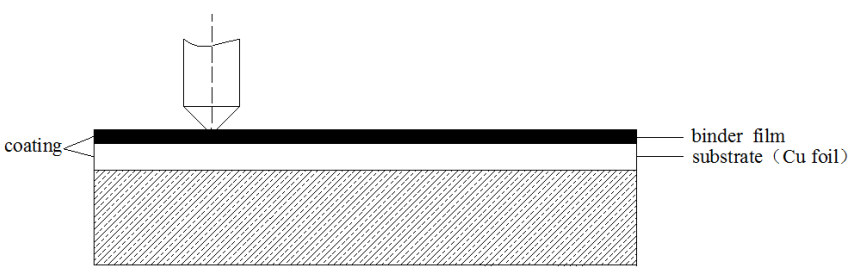

Figure 2. The mechanical model of coating scratch test.

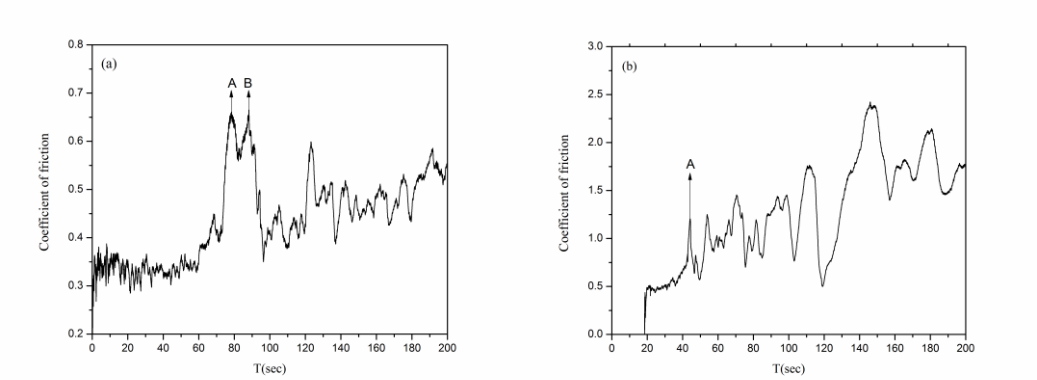

Figure 3. Coefficient of friction (COF) versus time curves of PVDF/Cu (a) and XG/Cu (b) coatings by scratching with a preload of 0.05N for 5s and then a linear load from 0.05N to 5N at a constant sliding speed of 0.04mm/s.

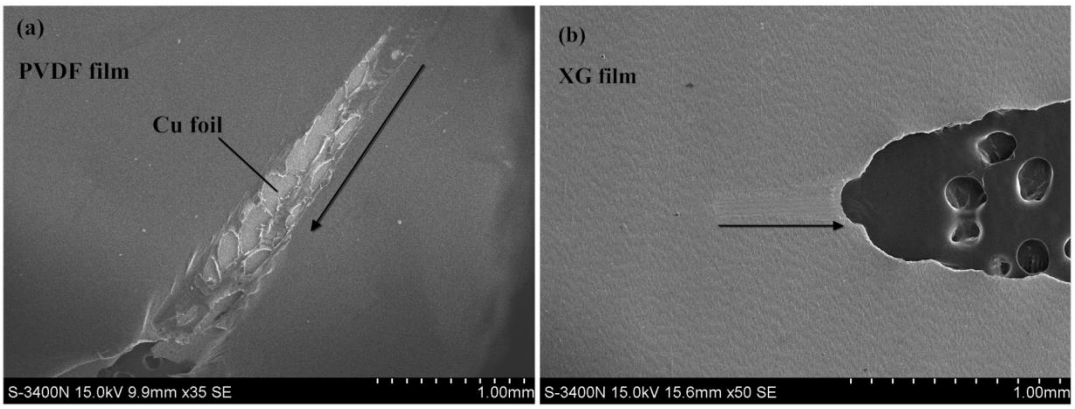

Figure 4. SEM images of the surface morphologies of PVDF/Cu (a) and XG/Cu (b) coatings after scratch tests;

Electrode adhesion strength is a relevant factor for Li-ion battery's development [45]. It is well recognized that the mechanical property plays a significant role to determine cycling performance. Better mechanical property is more beneficial to maintenance of a consistent electrically conducting network, leading to suppression of electrochemical grinding of solid-contents in electrode during the electrochemical process [46,47]. Fig.2 presents the mechanical model of coating scratch test. The composite coating consists of binder film and the Cu foil substrate. And the COF versus time curves of PVDF/Cu (a) and XG/Cu (b) coatings are displayed in Fig.3. The waves in coefficient of friction are corresponding to the surface of binder film yields and plastic deformation occurs along with the diamond tip apply stress on the sample surface. As seen in Fig.3.a, the coefficient of friction increases rapidly at point A for the first time which represents the complete fracture of PVDF film, then point B is corresponding to the crack of Cu foil substrate. The friction coefficient values are 0.659 and 0.653, respectively. While in Fig.3.b, the coefficient of friction increases rapidly at point A for the first time, representing the crack of holistic XG/Cu composite coating and the friction coefficient value is 1.192. The friction coefficient values affect a strong link between the hardness of polymer and the material flow around the diamond tip during scratching [35]. The crack of XG/Cu composite coating having a

higher friction coefficient value than PVDF/Cu composite coating implies the XG binder polymer has a larger hardness than PVDF with a further indication that the XG polymer has a larger plastic deformation resistance, which illustrates that the deformation occurs harder on XG binder. And the one less mutation of COF versus time curve of XG/Cu coating specimen is attributed to better adhesion between XG binder and Cu foil substrate than PVDF/Cu coating. The good adhesion strength of XG binder may arise from its abundant functional groups such as carboxyl and hydroxyl, which are naturally present and evenly distributed along the polymer chain. These functional groups contribute to a larger numbers of possible active bonding sites among active material, conductive agent and current collector, facilitating electronic and ionic conducting and ensuring good dispersion during the slurry production and electrode fabrication process [44].

To understand the above mechanical performance, the surface morphologies of PVDF/Cu (a) and XG/Cu (b) coatings after scratch tests were obtained using SEM in Fig.4.a and Fig.4.b. The arrow direction displays the scratch direction. With the diamond tip touches the specimens under a constant preload of 0.05N for 5s, the surface of coatings produces little deformation and stress. Then the PVDF/Cu and XG/Cu specimens undergo different crack process along with the diamond tip scratches over the coatings surface at a linear load from 0.05N to 5N. The crack process of the former included the elasto-plastic deformation of PVDF film, the incomplete crack and complete crack of PVDF film, finally the crack of Cu foil substrate, while the latter contained the elasto-plastic deformation of XG film, then the together crack of XG/Cu coating. It is clearly to see that the XG film doesn't crack when the diamond tip scratches over the coating surface, just with a scratch mark, which also demonstrate that the XG binder has a larger plastic deformation resistance than the PVDF binder as mentioned above.

3.2. Electrochemical performance

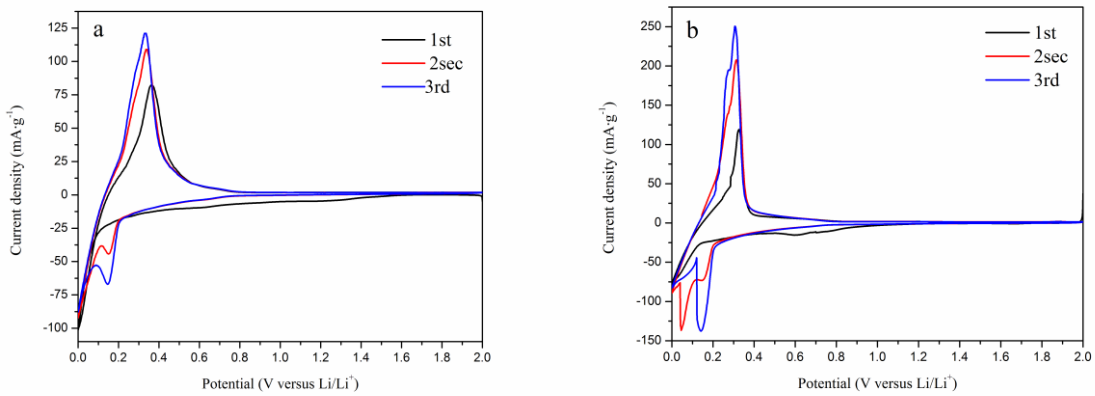

Figure 5. Cyclic voltammograms of the graphite anode coated with XG (a) and PVDF (b) at the scan rate of 0.1mV·s^{-1} between the potential of 0.0V and 2.0V (vs. Li/Li^{+}).

Fig.5 shows the CVs of the graphite anode coated with XG and PVDF binders in the initial three cycles. Obviously, the use of PVDF provides a reductive peak at around 0.7V corresponds to the solid electrolyte interface (SEI) formation reaction as it disappears for subsequent cycles, which results

the irreversible capacity loss. By contrast, the XG-based graphite anode exhibits a reduction peak ranging from 1.5V to 0.6V in the first cycle. These results imply that the kinetics of SEI formation will be different for the different choices of binders, and some previous reports have demonstrated that hydroxyl group and carboxyl group are beneficial to the formation of the SEI film [14, 48]. The formation of SEI film on the surface of anodes could promote the stability during the long-term cycling and facilitate the lithium ion conductivity.

In the following reduction process, the peaks at around 0.15V,0.05V correspond to the process of lithium intercalation to the graphite interlayer (Li_xC_6, $x \leq 1$). The oxidation peaks between 0.2V and 0.4V are related to the lithium de-intercalation from Li_xC_6. The PVDF-based electrode provides a lithium de-insertion potential of about 0.32V, and the use of XG shifts slightly to about 0.36V. The tiny difference may be caused by the reason that XG prefers to be ionic conductor. Refer to one previous report [41], XG showed a little higher lithium de-insertion potential than PVDF as a binder using for the mesocarbon microbeads (MCMBs) anode, which proved that XG performed negative shifts of the lithium de-insertion as the cellulose-based binder is electronic insulators but expected to be ionically more conductive. The binder adds a physical barrier to lithium insertion/de-insertion, which makes the lithium ion movement process more difficult than in the bare binder, while which are still expected to enhance the electrode/electrolyte interface.

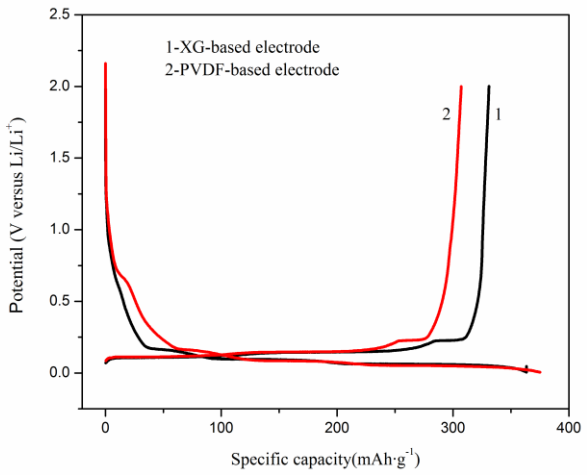

Figure 6. The first charge-discharge curves of the natural graphite electrodes fabricated with different binders between 0.5mV and 2.0V (vs. Li/Li^+) at the room temperature.

Fig.6 displays the first charge-discharge curves of the graphite electrodes with different binders. For the PVDF-based graphite electrode, the cell voltage drops quickly from the open circuit voltage (OCV) down to 0.75V, corresponding to the formation of solid electrode interface (SEI), and then the voltage decreased to about 0.2V, which indicates the lithium intercalation stage. Meanwhile, using XG as a binder, the formation of SEI happens at a higher voltage about 1.0V. The initial charge/discharge capacity of electrodes with PVDF and XG binders were 375/307, 363/331, $mAh \cdot g^{-1}$, respectively. Thus, the initial irreversible capacity and columbic efficiency are 62/81.9, 32/91.2, $mAh \cdot g^{-1}$/%, respectively. The graphite electrode with XG binder can attain well electrochemical

characteristics in the first cycle, which demonstrates that the reductive decomposition of the electrolyte components on the electrode/electrolyte surface is weaker than the electrode with PVDF binder.

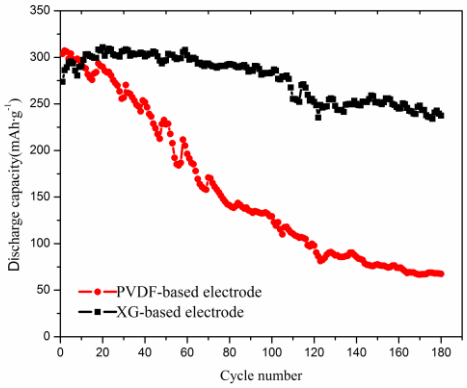

Figure 7. Discharge capacity of the natural graphite electrodes prepared with different binders at C/2 for 180 cycles between 5mV and 2V versus Li/Li^+.

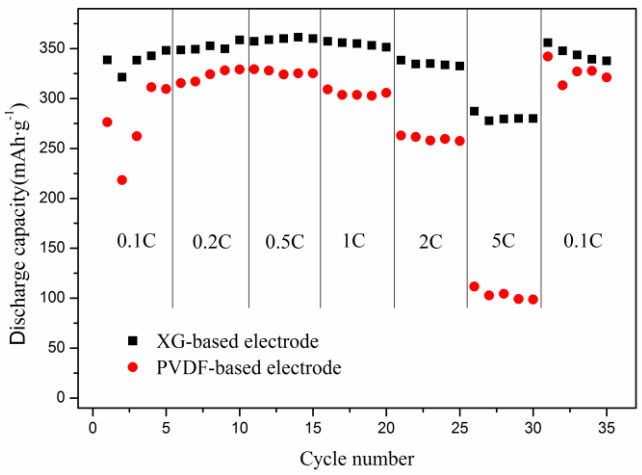

Figure 8. Rate capability of the natural graphite electrodes prepared with different binders, cycled between 5mV and 2V versus Li/Li^+ at different C-rates C/10, C/5, C/2, C, 2C, 5C, C/10.

It has been proved that hydroxyl and carboxylic functional groups contribute to improved cycle lifetime [31]. Fig.7 shows the cycle performance of the graphite anodes prepared with PVDF and XG binders at C/2 over 180 cycles. It is clearly to see that the discharge capacity profile of the graphite anode using PVDF binder shows a linear fall. The first discharge capacity is about 310 $mAh \cdot g^{-1}$, while the 180th discharge capacity drops to only 70 $mAh \cdot g^{-1}$. In the contrast, the discharge capacity of the graphite anode using XG binder is relatively stable. Before 60 cycles, the discharge capacity maintains above 300 $mAh \cdot g^{-1}$. Until 180th cycle, the discharge capacity is near 250 $mAh \cdot g^{-1}$. Based on these results, the graphite anode coated with XG binder shows a better electrochemical stability during the

electrochemical cycles, which can be explained by the better adhesive between the XG binder and Cu foil as well as the larger plastic deformation resistance that XG binder presents a better ability to resist deformation to buffer the graphite volume expansion during the long-term charge-discharge cycle tests that conforms to the mechanical property in the above discussion.

The rate capabilities of the graphite anodes prepared with PVDF and XG binders are investigated and the results are shown in Fig.8. After the three formation cycles at 20/C, all the batteries were charged (lithiated) at 5/C and followed by a discharge at different C rates (C/10, C/5, C/2, C, 2C, 5C, C/10). As shown in Fig.8, the cells with PVDF and XG binders show a similar performance, i.e. that the cells with PVDF and XG binders reach a maximum capacity at a rate of C/2, and the discharge capacity starts to drop at the rate of 1C. At the rate of 2C,the discharge capacity of XG-based electrode still remains above 300mAh·g^{-1},while the discharge capacity of PVDF-based electrodes about 250mAh·g^{-1}.But dramatically, cell capacity by using XG binder maintains 275 mAh·g^{-1} at a rate of 5C,yet the cell capacity by using PVDF binder drops to 100 mAh·g^{-1}.When the batteries cycled back at 10/C, the graphite anodes with PVDF and XG binders present a little higher capacity than the former at a rate of 10/C, which illustrates the batteries can't be fully activated at the initial five cycles at 10/C. The results demonstrate that the cell using XG binder shows a better high rate capability than the PVDF-based cell.

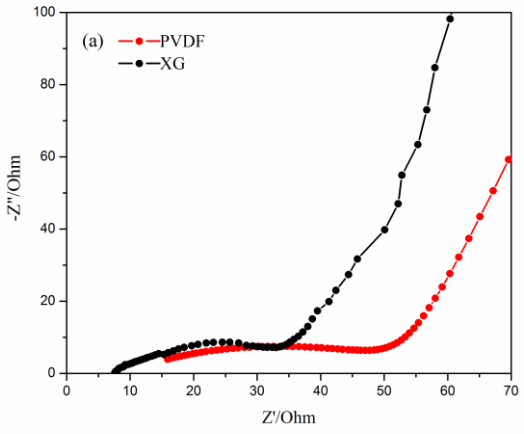

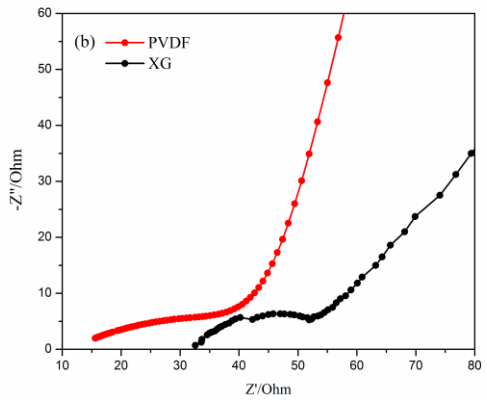

(c)

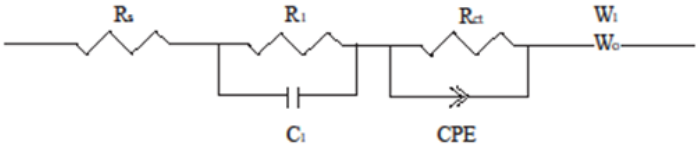

Figure 9. Nyquist plots of graphite electrodes using XG and PVDF binder from 10^{-2} to 10^{5} Hz at 100% DOD, (a) after 180 long-term cycles. (b) after different rates cycles (C/10, C/5, C/2, C, 2C, 5C, C/10). (c) the equivalent circuit used for the fitting of the EIS data.

Table 1. Charge transfer resistance Rct for graphite with XG and PVDF binders.

	Rct(Ω)	
binder	after different rates cycles	after 180 long-term cycles
PVDF	41.41	28.41
XG	17.55	28.37

The EIS technique has been an available tool for investigating the further electrode kinetics. Fig.9 displays the EIS of Li/graphite cell at 100% DOD after different cycling stages and an equivalent circuit used for modeling the spectrum. Definitely, the EIS consists of two semicircles. As discussed before [5, 49, 50], each semicircle can be fitted by an analogous equivalent circuit. Rs represents the resistance of the solution. The high-frequency semicircle is considered as the resistance (R_1) of passivating SEI film, and medium-frequency semicircle reflects the charge-transfer resistance (Rct) at the electrodes.C_1 and CPE are the capacity and constant phase element associated with R_1 and Rct, respectively. The inclined line at the low frequency is related to be the Warburg impedance of a diffusion process of Li^+ ion in the electrolyte-electrode interface. In this work, the values of parameter Rct after a least squares fitting were summarized at Table.1. As shown in Table 1, graphite with XG binder has the smaller Rct values than those of PVDF binder after different cycle stages, indicating the enhancement in the kinetics in the rate and long-term cycle capacities of XG-based graphite anode, i.e. more ion transport and charge-transfer sites happens at the electrode-electrolyte interface during the lithiation/delithiation process that corresponds to cyclic voltammetry experiment in Fig.5., also the theory could be proved in He's report [44]. The binder may affect the electrolyte permeation inside the composite material, thereby favoring Li^+ transport but also enhancing the electrolyte reactions on active particles [50]. High Li^+ ionic conductivity will facilitate the fast ion transport especially beneficial for high rate operation [51], so XG-based cell owns a better high rate capability than the PVDF-based cell as shown in Fig.8. The high electrolyte uptake is beneficial for high Li^+ diffusion efficiency and subsequently facilitates the high capacity and better power performance of the electrode [31]. The lower impedance confirms that the electrode with XG binder has a relatively stable surface

condition after different cycle stages. On the basis of these analyses, XG presents apparent advantages in fabricating high-performance anode compared with conventional PVDF binder.

4. CONCLUSIONS

The natural graphite electrode fabricated with XG binder presented a remarkable electrochemical performance. Compared with the conventional PVDF-based anode, the initial columbic efficiency, cycling stability and rate capability were substantially improved. The wear tests were not only to demonstrate that the XG film has a higher elasticity than the PVDF film, but also to prove that there is better adhesion strength between XG binder and Cu foil substrate than PVDF/Cu coating. EIS measurements manifested that the graphite electrode using XG as binder had lower charge transfer resistance and more active kinetics on the electrode/electrolyte surface than the electrode using PVDF binder. The present results indicate that the graphite electrode with XG as binder not only can reduce cost and environmental pollution, but also can enhance the electrochemical performance. All the test results are in accordance with the former study.

References

1. J. M. Tarascon, M. Armand, *Nature*, 414 (2001) 359.
2. M. Hu, X. L. Pang, Z. Zhou, *J. Power Sources*, 237 (2013) 229.
3. J. B. Goodenough, Y. Kim, *Chem. Mater*, 22 (2010) 587.
4. S. L. Chou, J. Z. Wang, H. K. Liu, S. X. Dou, *J. Phys. Chem. C.*, 115 (2011) 16220.
5. Z. Fu, H. L. Feng, X. D. Xiang, M. M. Rao, W. Wu, J. C. Luo, T. T. Chen, Q. P. Hu, A. B. Feng, W. S. Li, *J. Power Sources*, 261 (2014) 170.
6. G. Liu, H. Zheng, A. S. Simens, A. M. Minor, X. Song, V. S. Battaglia, *J. Electrochem. Soc.*,154 (2007) A1129.
7. M. Mancini, F. Nobili, R. Tossici, R. Marassi, *Electrochim. Acta*, 85 (2012) 566.
8. J. Xu, S. L. Chou, Q. F. Gu, H. K. Liu, S. X. Dou, *J. Power Sources*, 5 (2013) 172.
9. Y. S. Park, E. S. Oh, S. M. Lee, *J. Power Sources*, 248 (2014) 1191.
10. L. Qiu, Z. Q. Shao, D. X. Wang, W. J. Wang, F. J. Wang, J. Q. Wang, *Carbohyd. Polym.*, 111 (2014) 588.
11. J. T. Xu, S. L. Chou, Q. F. Gu, H. K. Liu, S. X. Dou, *J. Power Sources*, 225 (2013) 172.
12. M. H. T. Nguyen, E. S. Oh, *J. Electroanal Chem.*, 739 (2015) 111.
13. J. Pan, G. Y. Xu, B. Ding, Z. Chang, A. X. Wang, H. Dou, X. G. Zhang, RSC Adv., 6 (2016) 40650
14. H. K. Park, B. S. Kong, E. S. Oh, *Electrochem. Commun.*, 13 (2011) 1051.
15. P. P. Prosini, M. Carewska, C. Cento, A. Masci, *Electrochim. Acta*, 150 (2014) 129.
16. J. Bae, S. H. Cha, J. Park, *Macromol Res.*, 21 (2013) 826.
17. J. S. Kim, W. Choi, K. Y. Cho, D. Byun, J. C. Lim, J. K. Lee, *J. Power Sources*, 244 (2013) 521.
18. L. L. Chai, Q. T. Qu, L. F. Zhang, M. Shen, L. Zhang, H. H. Zheng, *Electrochim. Acta*, 105 (2013) 378.
19. H. Zhao, X. Zhou, S. J. Park, F. F. Shi, Y. B. Fu, M. Ling, N. Yuca, V. S. Battaglia, G. Liu, *J. Power Sources*, 263 (2014) 288.
20. D. V. Carvalho, N. Loeffler, G-T. Kim, M. Marinaro, M. W-Mehrens, S. Passerini, *Polymers*, 8 (2016) 276.

21. Q. Y. Li, H. J. Yang, L. S. Xie, J. Yang, Y. N. Nuli, J. L. Wang, *Chem. Commun.*, 52 (2016) 13479.
22. M. Y. Wu, X. C. Xiao, N. Vukmirovic, S. D, Xun, P. K. Das, X. Y. Song, P. O. Velasco, D. D. Wang, A. Z. Weber, L. W. Wang, V. S. Battaglia, W. L. Yang, G. Liu, *J. Am. Chem. Soc.*, 135 (2013) 12048.
23. Q. F. Yuan, F. G. Zhao, Y. M. Zhao, Z. Y. Liang, D. L. Yan, *J. Solid. State. Electr*ochem., 18 (2014) 2167.
24. L. B. Chen, X. H. Xie, J. Y. Xie, K. Wang, J. Yang, *J. Al. Electrochem.*, 36 (2006) 1099.
25. M. H. Ryou, J. Kim, I. Lee, S. Kim, Y. K. Jeong, S. Hong, J. H. Ryu, T. S. Kim, J.K. Park, H. Lee, J. W. Choi, *Adv. Mater*, 25 (2013) 1571.
26. K. Krzysztof. *J. Mater. Eng. Perform.*, 25(2016) 2326.
27. T. Yim, S. J. Choi, Y. N. Jo, T. H. Kim, K. J. Kim, G. Jeong, Y. Kim, *Electrochim. Acta*, 136 (2014) 112.
28. J. Yoon, D. X. Oh, C. Jo, J. Lee, D. S. Hwang, *Phys. Chem. Chem. Phys*., 16 (2014) 25628.
29. H. Zheng, R. Z. Yang, G. Liu, X. Y. Song, V. S. Battaglia, *J. Phys. Chem.* C, 116 (2012) 4875.
30. N. Yuca, H. Zhao, X. Y. Song, M. F. Dogdu, W. Yuan, Y. B. Fu, V. S. Battaglia, X. C. Xiao, G. Liu, *ACS Al. Mat. Interfaces*, 6 (2014) 17111.
31. M. Ling, Y. N. Xu, H. Zhao, X. X. Gu, J. X. Qiu, S. Li, M. Y. Wu, X. Y. Song, C. Yan, G. Liu, S. Q. Zhang, *Nano Energy*, 12 (2015) 178.
32. M. Yoo, C. W. Frank, S. Mori, S. Yamaguchi, *Polymer*, 44 (2003) 4197.
33. S. Ramdon, B. Bhushan, *J. Power Sources*, 246 (2014) 219.
34. D. Dong, X. H. Chen, W. T. Xiao, G. B. Yang, P. Y. Zhang, *Al. Surf Sci*, 255 (2009) 7051.
35. P. F. Li, H. Zhou, X. H. Cheng, *Al. Surf Sci*, 285P (2013) 937.
36. M. Ö. Bora, *Tribol. Int*., 78 (2014) 75.
37. P. Kurkcu, L. Andena, A. Pavan, *Wear*, 317 (2014) 277.
38. H. K. Park, B. S. Kong, E. S. Oh, *Electrochem. Commun*., 13 (2011) 1051.
39. L. Y. Gong, M. H. T. Nguyen, E. S. Oh, *Electrochem. Commun*., 29 (2013) 45.
40. Z. Xue, Z. C. Zhang, K. Amine, *Electrochem. Commun*., 34 (2013) 86.
41. F. M. Courtel, S. Niketic, D. Duguay, Y. A. Lebdeh, I. J. Davidson, *J. Power Sources*, 196(2011) 2128.
42. N. Cuesta, A. Ramos, I. Cameán, C. Antuña, A. B. García, *Electrochim. Acta*, 155 (2015) 140.
43. D. Chen, R. Yi, S. R. Chen, T. Xu, M. L. Gordin, D, H. Wang, *Solid State Ionics*, 254 (2014) 65.
44. J. R. He, H. X. Zhong, J. L. Wang, L. Z. Zhang, *J. Alloys Compd., 714* (2017) 409.
45. W. Haselrieder, B. Westphal, H. Bockholt, A. Diener, S. HÖft, A. Kwade, *Int. J. Adhes. Adhes.*, 60 (2015) 1.
46. S. D. Beattie, D. Larcher, M. Morcrette, B. Simon, J. M. Tarascon, *J. Electrochem. Soc.*, 155 (2008) A158.
47. D. Mazouzi, B. Lestriez, L. Roué, D. Guyomard, *Electrochem. Solid. ST.*, 12 (2009) A215.
48. S. Komaba, N. Yabuuchi, T. Qzeki, K. Okushi, H. Yui, K. Konno, Y. Katayama, T. Miura, *J. Power Sources*, 195(2010) 6069.
49. S.S.Zhang, M.S.Ding, K.Xu, J.Allen, T.R.Jow, *Electrochem. Solid-State Lett*., 4 (2001) A206.
50. F. Bigoni, F. D. Giorgio, F. Soavi, C. Arbizzani, *J. Electrochem. Soc.*, 164 (2017) A6171.
51. Y. G. Cho, Y. S. Kim, D. G. Sung, M. S. Seo, H. K. Song, *Energy Environ. Sci.*, 7 (2014) 1737.